Protein Science (1999), *8*:800–809. Cambridge University Press. Printed in the USA.

The use of dipolar couplings for determining the solution structure of rat apo-S100B($\beta\beta$)

ALEXANDER C. DROHAT,[1] NICO TJANDRA,[2] DONNA M. BALDISSERI,[1] AND DAVID J. WEBER[1]

[1]Department of Biochemistry and Molecular Biology, University of Maryland School of Medicine, 108 North Greene Street, Baltimore, Maryland 21201
[2]Laboratory of Biophysical Chemistry, Building 3, Room 418, National Heart, Lung, and Blood Institute, National Institutes of Health, Bethesda, Maryland 20892-0380

(RECEIVED November 4, 1998; ACCEPTED December 30, 1998)

Abstract

The relative orientations of adjacent structural elements without many well-defined NOE contacts between them are typically poorly defined in NMR structures. For apo-S100B($\beta\beta$) and the structurally homologous protein calcyclin, the solution structures determined by conventional NMR exhibited considerable differences and made it impossible to draw unambiguous conclusions regarding the Ca^{2+}-induced conformational change required for target protein binding. The structure of rat apo-S100B($\beta\beta$) was recalculated using a large number of constraints derived from dipolar couplings that were measured in a dilute liquid crystalline phase. The dipolar couplings orient bond vectors relative to a single-axis system, and thereby remove much of the uncertainty in NOE-based structures. The structure of apo-S100B($\beta\beta$) indicates a minimal change in the first, pseudo-EF-hand Ca^{2+} binding site, but a large reorientation of helix 3 in the second, classical EF-hand upon Ca^{2+} binding.

Keywords: Ca^{2+}-binding protein; dipolar coupling; EF-hands; NMR; S100 proteins; S100β; S100B; three-dimensional structure

A Ca^{2+}-dependent conformational change in S100B($\beta\beta$) is required for it to bind most effector proteins (Kligman & Hilt, 1988). While the precise mechanism for intra- and extracellular functions of S100B($\beta\beta$) are not well understood, processes such as cell growth, energy metabolism, protein phosphorylation, apoptosis, and Ca^{2+} signaling are regulated via S100B($\beta\beta$) (Donato, 1991; Zimmer et al., 1995; Schafer & Heizmann, 1996). Interestingly, several target proteins of S100B($\beta\beta$) are substrates of kinase-dependent phosphorylation reactions. For example, S100B($\beta\beta$) inhibits the protein kinase C-dependent (PKC) phosphorylation of the MARCKS protein (myristoylated alanine-rich C-kinase substrate) (Patel & Kligman, 1987; Stumpo et al., 1989), S100 modulated phosphoprotein (SMP) (Patel et al., 1983), the glial fibrillary acidic protein (GFAP) (Bianchi et al., 1993), neuromodulin (Baudier et al., 1989), and the negative cell cycle regulator protein (p53) (Baudier et al., 1992; Rustandi et al., 1998; Wilder et al., 1998). For neuromodulin, MARCKS, and p53, it has been shown that S100B($\beta\beta$) binds the substrate prior to phosphorylation and sterically prevents catalysis (Baudier et al., 1992; Rustandi et al., 1998; Wilder et al., 1998). Although calmodulin also binds and inhibits phosphorylation of MARCKS (Albert et al., 1984) and neuromodulin (Baudier et al., 1989), for neuromodulin this interaction is Ca^{2+} independent (Urbauer et al., 1995), and for GFAP and p53, calmodulin has no inhibitory effect (Baudier et al., 1992; Bianchi et al., 1993). In addition, S100B($\beta\beta$) cannot activate most calmodulin-dependent enzymes or proteins. Thus, the biological functions of S100B($\beta\beta$) are clearly distinct from those of calmodulin (Zimmer et al., 1995).

Like calcyclin and other members of the S100 protein family (Potts et al., 1995; Zimmer et al., 1995), S100B($\beta\beta$) is a dimer with each S100β subunit containing two helix-loop-helix Ca^{2+} binding domains now referred to as the "typical" and "pseudo" EF-hand motifs, respectively (Kligman & Hilt, 1988; Strynadka & James, 1989; Amburgey et al., 1995a; Potts et al., 1995) (Fig. 1). The pseudo-EF hand was given its name because it has 14 rather than 12 residues, and it generally binds Ca^{2+} with lower affinity than the typical EF-hand (Kligman & Hilt, 1988). The three-

Reprint requests to: David J. Weber, Department of Biochemistry and Molecular Biology, University of Maryland School of Medicine, 108 North Greene Street, Baltimore, Maryland 21201; e-mail: dweber@umaryland.edu.

Abbreviations: DHPC, dihexanoyl phosphatidylcholine; DMPC, dimyristoyl phosphatidylcholine; DTT, dithiothreitol; GFAP, glial fibrillary acidic protein; HSQC, heteronuclear single quantum coherence; IPAP, in-phase anti-phase; LC, liquid crystalline; MARCKS, myristoylated alanine-rich kinase C substrate protein; NOE, nuclear Overhauser effect; NOESY, NOE spectroscopy; NMR, nuclear magnetic resonance; PDB, Protein Data Bank; PKC, protein kinase C; RMSD, root-mean-square difference; ROESY, rotating frame Overhauser effect spectroscopy; S100β, subunit of dimeric S100B; S100B($\beta\beta$), dimeric S100B with noncovalent interactions at the dimer interface; S100B(β-β) dimeric S100B with disulfide bonds at the dimer interface; SMP, S100 modulated protein; 2D, two-dimensional; 3D, three-dimensional; 4D, four-dimensional; TPPI time-proportional phase incrementation.

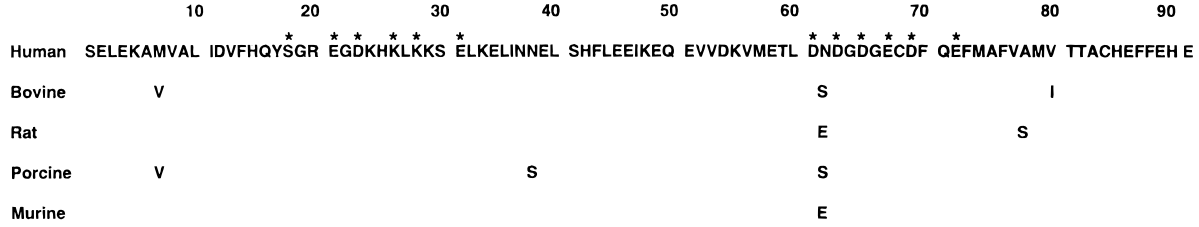

Fig. 1. Sequence homology of the S100β subunit from several mammalian species. Only amino acids that differ from the human S100β sequence are shown. The amino acid residues that are involved in the pseudo- and typical EF-hand Ca^{2+} binding domains are indicated by asterisks.

dimensional structures of Ca^{2+}-bound S100B($\beta\beta$) and calcyclin confirmed the presence of the EF-hand binding domains (Drohat et al., 1998; Matsumura et al., 1998; Sastry et al., 1998; Smith & Shaw, 1998), and a comparison of the Ca^{2+}-bound structures to those of the apo-form becomes important for understanding how S100 proteins function in solution. However, a discrepancy regarding the position of helix 3 in the apo-structures of S100B($\beta\beta$) from different sources (rat, bovine; Fig. 1) and calcyclin has led to confusion regarding the extent of the conformational change that occurs for dimeric S100 proteins upon the addition of Ca^{2+} (Potts et al., 1995; Drohat et al., 1996; Kilby et al., 1996).

Unambiguous information defining the orientation of helix 3 with respect to the remainder of the S100B homodimer can be obtained from the measurement of one-bond dipolar couplings when the protein is dissolved in a dilute lyotropic liquid crystalline phase of phospholipid bicelles. Here we report the structure of apo-S100B($\beta\beta$), calculated with the inclusion of dipolar coupling restraints. The true position of helix 3 is found to lie between that reported previously for rat and bovine apo-S100B($\beta\beta$) (Drohat et al., 1996; Kilby et al., 1996) and differs substantially from that of a preliminary, low-resolution structure of apo-calcyclin (Potts et al., 1995). Comparison of the apo-S100B($\beta\beta$) structure determined here with the recently determined structures of Ca^{2+}-bound S100B($\beta\beta$) (Drohat et al., 1998; Matsumura et al., 1998; Smith & Shaw, 1998) reveals a large change in the orientation of helix 3 upon Ca^{2+} ligation.

Results and discussion

As with most NMR structures, the apo-S100 protein structures (i.e., S100B and calcyclin) were defined primarily by a large number of NOE-derived short-range (<5 Å) interproton distance constraints, supplemented by dihedral constraints derived from J couplings, and refined on the basis of ^{13}C chemical shift data (Potts et al., 1995; Drohat et al., 1996; Kilby et al., 1996). The cumulative effect of errors in NOE-derived interproton distances can make it very difficult to accurately define the relative orientation of structural elements that are connected by few NOEs (Clore et al., 1995). This constitutes the basis for the high degree of uncertainty in the location of helix 3 and for the large differences found in the orientation of this helix by different groups. As discussed extensively by Groves et al. (1998), accurate knowledge of the orientation of helix 3 in the apo-state is pivotal for understanding how Ca^{2+} ligation of S100B($\beta\beta$) modulates target protein binding. Dipolar couplings are uniquely suited to provide an unambiguous answer to this question and, therefore, we have measured a large number of such dipolar coupling constraints. As discussed below, dipolar couplings between nuclei separated by one or two bonds (i.e., at known internuclear distance) provide direct information on the orientation of the internuclear bond vector relative to the protein's alignment tensor **A**. As all these dipolar couplings define the corresponding interatomic vectors relative to a single axis system (the principal axis system of **A**), the relative orientation of structural elements is determined accurately by dipolar couplings, regardless of their separation in the three-dimensional structure.

Measurement of dipolar coupling values for S100B(ββ)

Measurement of dipolar couplings for S100B($\beta\beta$) relies on the same procedure originally used by Tolman et al. for myoglobin, in which the dipolar couplings were extracted from the change in J splitting as a function of the minute changes in molecular alignment with magnetic field strength (Tolman et al., 1995). Much larger and adjustable degrees of alignment can be obtained by dissolving the protein in a dilute nematic liquid crystalline phase (Bax & Tjandra, 1997; Tjandra & Bax, 1997a), containing magnetically oriented disc-shaped phospholipid particles, commonly referred to as bicelles (Sanders, 1992). The higher degree of alignment makes it possible to measure not only the one-bond $^1D_{N-H}$ and $^1D_{C\alpha-H\alpha}$ dipolar couplings, but also the much smaller $^1D_{C'-C\alpha}$, $^1D_{C'N}$, and two-bond $^2D_{C'-HN}$ interactions.

In the absence of decoupling, the observed splitting between two nuclei P and Q corresponds to the sum of the scalar and dipolar interactions, J_{PQ} and D_{PQ}. J_{PQ} is to a very good approximation independent of alignment, and D_{PQ} is simply obtained from the difference between the P–Q splitting measured in the aligned and isotropic phases. $^1D_{N-H}$ values are measured most easily from a [^{15}N–^1H]–2D correlation spectrum recorded in the absence of ^1H decoupling during the t_1 evolution period (Fig. 2A). To avoid the increase in spectrum complexity caused by the splittings, the upfield and downfield components of the ^{15}N–{$^1H^N$} doublets were separated into two spectra, recorded in an interleaved manner (Ottiger et al., 1998), but for clarity their superposition is shown in Figure 2A. The $^1D_{C\alpha-H\alpha}$ value is obtained most easily from the 3D (H)CA(CO)NH spectrum, recorded in the absence of ^1H decoupling during the C^α evolution period using the same pulse sequence that was used recently for measuring $^{13}C^\alpha$ anisotropy from relaxation interference (Tjandra & Bax, 1997b). The 3D spectrum is well dispersed and yields high resolution in the $^{13}C^\alpha$ dimension, permitting accurate measurement of $^1D_{C\alpha-H\alpha}$ (Fig. 2D). $^1D_{C'-C\alpha}$ values are simply obtained from recording the highly sensitive HNCO experiment (Grzesiek & Bax, 1992) without $^{13}C^\alpha$ decoupling during $^{13}C'$ evolution. The relatively narrow line width of

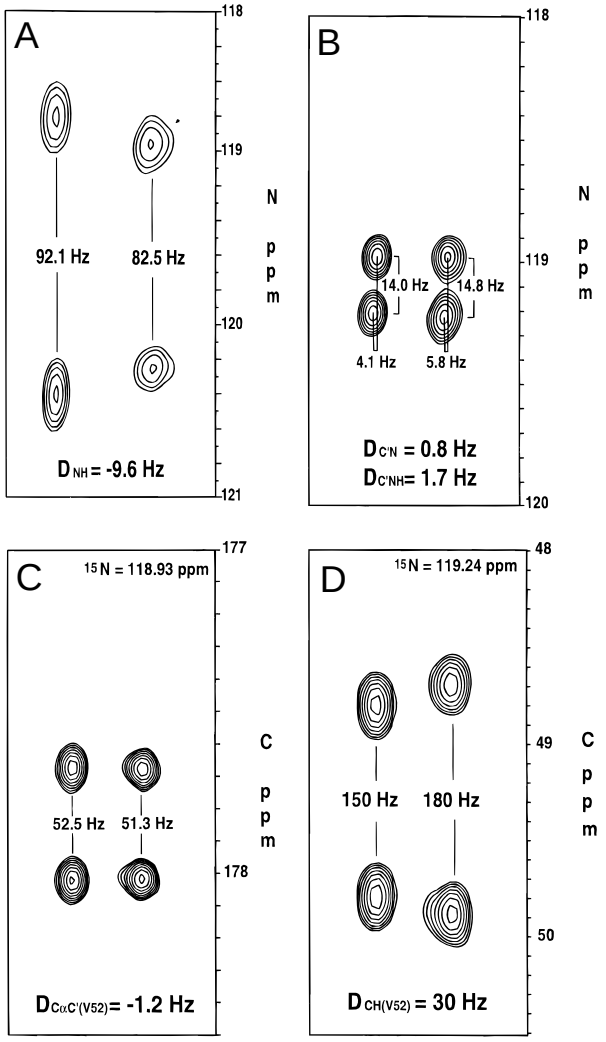

Fig. 2. Representative (**A**,**B**) 2D and (**C**,**D**) 3D spectra used to measure dipolar coupling values for pairs of resonances in rat apo-S100B($\beta\beta$). **A:** Small region of a 2D ^{1}H-^{15}N HSQC spectrum of rat apo-S100B($\beta\beta$) illustrating splittings for residues in helix 3 (V52, V53). Dipolar couplings were determined by comparing ^{1}H–^{15}N splittings recorded in the presence (right) and absence (left) of dilute liquid crystalline media. **B:** Likewise, dipolar coupling were determined using data from the constant time 2D ^{1}H–^{15}N HSQC spectra with ^{13}C′ coupling to N and H^{N} in anisotropic (right) and isotropic (left) samples. **C**,**D:** ^{15}N planes from (**C**) 3D CT-HNCO with C$^{\alpha}$-C′ coupling and from (**D**) 3D (H)CA(CO)NH with H$^{\alpha}$ to C$^{\alpha}$ coupling that illustrate the H^{N} of V53 and the splittings from V52. Dipolar couplings for the C$^{\alpha}$–C′ of V52 and H$^{\alpha}$–C$^{\alpha}$ of V52 were determined by comparing the splitting in the presence (right) or absence (left) of liquid crystalline media (**C**,**D**). Other conditions are as described in Materials and methods.

^{13}C′ again ensures accurate measurement of $^{1}D_{C'-C\alpha}$ (Fig. 2C). Finally, $^{1}D_{C'-N}$ and $^{2}D_{C'-HN}$ are both obtained from a single [^{15}N–^{1}H]–2D correlation spectrum, recorded in the presence of composite pulse decoupling during t_1 for obtaining the highest possible resolution (Ottiger et al., 1998). The difference in F_1 splitting (Fig. 2D) corresponds to $^{1}D_{C'-N}$, and the change in F_2 splitting yields $^{2}D_{C'-HN}$. The number of resonances in this 2D spectrum is doubled relative to that of a regular [^{15}N–^{1}H] correlation spectrum and accurate dipolar couplings could only be extracted for the very well-resolved resonances (about 50%).

Use of dipolar coupling values in the determination of the apo-S100B($\beta\beta$) structure

Dipolar couplings between two nuclei, P and Q, contain information regarding the orientation of their internuclear vector relative to the molecular alignment tensor such that

$$D_{PQ}(\theta,\phi) = \mathbf{S}(\mu_0/4\pi)\gamma_P\gamma_Q h\{A_a(3\cos^2\theta - 1) + \tfrac{3}{2}A_r \sin^2\theta\cos 2\phi\}/4\pi^2 r_{PQ}^3 \quad (1)$$

where **S** is the generalized order parameter for internal motion of the vector PQ, γ_P and γ_Q are the gyromagnetic ratios of P and Q, h is Plank's constant, r_{PQ} is the distance between P and Q, and θ and ϕ are the cylindrical coordinates describing the orientation of the PQ vector in the principal axis system of **A** (Tjandra & Bax, 1997a). Values for the axial (A_a) and rhombic (A_r) components of **A** depend on the shape of the protein and vary with the bicelle concentration, which is adjusted to yield an A_a of $\sim 10^{-3}$ (Bax & Tjandra, 1997). As with ubiquitin, there is a sufficient amount of space between individual bicelles, such that rotational diffusion and transverse relaxation rates are not significantly affected, and thus high resolution data with normal linewidths were obtained for apo-S100B($\beta\beta$) (Fig. 2).

Geometric information contained in the dipolar couplings was used during a simulated annealing protocol for structure calculations, which minimizes the difference between the measured dipolar couplings and those predicted by the structure (Tjandra et al., 1997; Clore et al., 1998b). Inclusion of dipolar constraints in the structure calculation required that we reevaluate the NOE constraints used in our earlier structure determination (Drohat et al., 1996). In particular, one very weak contour, thought to be an NOE from A75C$^{\beta}$H$_3$–V52C$^{\gamma}$H$_3$, gave a large violation when the dipolar coupling constraints were added. This contour turned out to be an artifact, and its previous inclusion in the structure calculation contributed significantly to the orientation of helix 3. When this constraint was removed, the dipolar coupling and the remaining NOE constraints agreed within error with our newly calculated structures. In addition, a large number of other weak and very weak NOE constraints that were ambiguous based on chemical shift values were removed initially. However, most (>99%) of these weak NOE correlations were intraresidue or sequential NOEs, and they could generally be added back to the structure calculation without violating the newly added dipolar coupling constraints.

Solution structure of rat apo-S100B($\beta\beta$) and comparison to earlier S100 structures

Over 500 long-range dipolar coupling constraints were included in the structure calculation of apo-S100B($\beta\beta$) (Fig. 3). These constraints, together with 316 intraresidue, 538 sequential, 538 medium-range, 278 long-range, and 108 intermolecular NOE-derived distance constraints, plus 330 dihedral and 176 hydrogen bond constraints were used to calculate the structure of apo-S100B($\beta\beta$) (Table 1). Figure 4A illustrates the superposition (C$_{\alpha}$) of the final 20 structures, which are well converged with a root-mean-square difference (RMSD) from the mean structure of 0.29 Å for backbone atoms in residues 1–84 and 0.99 Å for all heavy atoms in residues 1–84, and low RMSDs from the experimental constraints and idealized covalent geometry (Table 1). The resolution of the refined structure is much better than those of the previously deter-

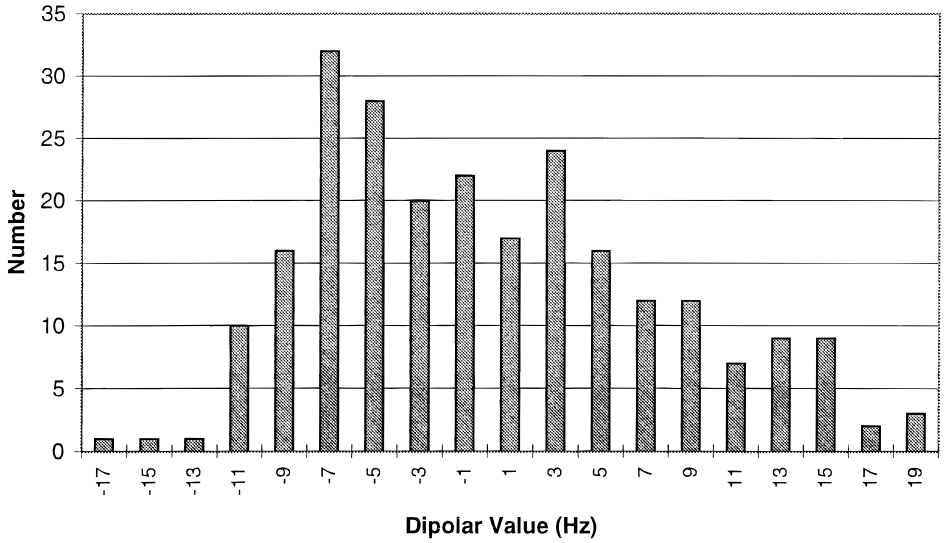

Fig. 3. Distribution of all the dipolar coupling values used to determine the structure of rat apo-S100B($\beta\beta$). The data are normalized to the D_{NH} data based on bond lengths and gyromagnetic ratios as previously described (Clore et al., 1998a).

mined structures of rat apo-S100B($\beta\beta$) (^{backbone}RMSD = 1.04 Å; ^{heavy}RMSD = 1.62 Å), bovine apo-S100B($\beta\beta$) (^{backbone}RMSD = 1.26 Å; ^{heavy}RMSD = 1.76 Å), and apo-calcyclin (^{backbone}RMSD = 2.72 Å; ^{heavy}RMSD = 3.19 Å) (Potts et al., 1995; Drohat et al., 1996; Kilby et al., 1996). The 20 structures have an average of 86% of the residues in the most favorable region of the Ramachandran plot, and no structure has residues in the disallowed regions that is significantly better than previous structures of rat apo-S100B($\beta\beta$) (76% in most favored region), bovine apo-S100B($\beta\beta$) (70%), and calcyclin (65%) (Potts et al., 1995; Drohat et al., 1996; Kilby et al., 1996). The lowest energy member of the newly calculated ensemble of rat apo-S100B($\beta\beta$) structures exhibits the lowest RMSD from the mean structure, has the largest number of residues in the most favorable region of the Ramachandran diagram (88%), and has better than average values for all other measures of quality using the program PROCHECK (Laskowski et al., 1993). The quality of the structure was also evaluated using the recently proposed *Q* factor approach (Cornilescu et al., 1998; Ottiger & Bax, 1998). In this evaluation, the agreement between dipolar couplings predicted by the structure and those measured, but not included in the structure calculation, is expressed by the factor *Q*:

$$Q = \left[\sum_{i=1,\ldots,N} (D_{CHi}^{meas} - D_{CHi}^{pred})^2/N \right]^{1/2} \Big/ D^{RMS} \qquad (2)$$

where the summation extends over all *N* residues for which $^{13}C^{\alpha}$–$^{1}H^{\alpha}$ dipolar couplings (D_{CHi}) could be measured. D^{RMS} is the root-mean-square value of the measured D_{CHi} couplings. D_{CHi}^{pred} corresponds to the predicted $^{13}C^{\alpha}$–$^{1}H^{\alpha}$ dipolar coupling when the orientation and magnitude of the alignment tensor are optimized to yield best agreement between measured couplings and the protein structure (Tjandra et al., 1996). Thus, the atomic coordinates used to calculate D_{CHi}^{pred} are from a protein structure that is determined using all of the NMR-derived constraints except the D_{CH} couplings. This *Q*-factor is somewhat analogous to the free *R*-factor, commonly used to evaluate X-ray crystal structures (Brünger et al., 1993). It should be noted that the dipolar coupling is a rather steep function of the internuclear vector orientation, and *Q*-factors tend to be considerably higher than free *R*-factors used in crystallography. For example, *Q* factors for the previous structures of rat apo-S100B($\beta\beta$), bovine apo-S100B($\beta\beta$), and calcyclin are 0.62, 0.68, and 0.90, respectively; whereas the new structure yields a quality factor of $Q = 0.36$ when both the $^{1}D_{NH}$ and $^{1}D_{CH}$ quality factors are considered together as a weighted average.

The structure of apo-S100B($\beta\beta$) was also calculated without the use of the dipolar coupling constraints, but with the final set of accurate NOE and scalar coupling constraints included. In these structures, the quality factor ($^{1}D_{NH}$ and $^{1}D_{CH}$) dropped from $Q = 0.36$ to $Q = 0.49$, and the RMSD for backbone (residues 2–84) increased from 0.29 to 0.57 Å. Nonetheless, while the quality decreased for the protein structure calculated with only the NOE and scalar coupling constraints, it did have the same interhelical angles as the structures calculated with dipolar couplings included (data not shown). In addition, the pairwise RMSD between the average structures calculated with and without dipolar coupling constraints is slightly less than 0.57 Å, indicating that the two families of structures are indistinguishable.

When previously determined structures of apo-S100 proteins are compared to the refined structure of apo-S100B($\beta\beta$) that includes dipolar couplings, there are large RMSDs in backbone C^{α}, particularly with regard to the position of helix 3 (Table 2). These discrepancies are further manifested by different helix 3/helix 4 interhelical angles for each of the proteins ($\Omega_{3/4}$) ($^{rat\ S100B}\Omega_{3/4} = 220 \pm 4$ (Drohat et al., 1996); $^{bovine\ S100B}\Omega_{3/4} = 164 \pm 4$ (Kilby et al., 1996); $^{calcyclin}\Omega_{3/4} = 145 \pm 16$ (Potts et al., 1995) (Table 3). Because of these discrepancies, our ability to determine the extent of the conformational change observed in S100 proteins upon the addition of Ca^{2+} have been limited. However, the inclusion of stringent long-range constraints derived from dipolar coupling data has resolved this problem (Fig. 4), and the orientation of helix 3 ($^{new}\Omega_{3/4} = 194 \pm 1$) is now in between that found previously for the structures of apo-S100B from rat and bovine (Fig. 4B), and

Table 1. *Structural statistics* [a]

	20	Best
RSMDs from experimental distance restraints (Å)		
All distance restraints (1,954)	0.013 ± 0.001	0.012
Intraresidue (316)	0.011 ± 0.003	0.007
Sequential ($\|i - j\| = 1$) (538)	0.015 ± 0.001	0.015
Medium-range ($1 < \|i - j\| \leq 5$) (538)	0.011 ± 0.001	0.013
Long-range ($\|i - j\| > 5$) (278)	0.010 ± 0.002	0.009
Intermolecular (108)	0.010 ± 0.002	0.008
Hydrogen bonds (176)	0.019 ± 0.004	0.016
RMSDs from dipolar coupling restraints (Hz)		
$^1D_{NH}$ (64)	1.46 ± 0.05	1.54
$^1D_{NH}$ cat.2 (44)	2.61 ± 0.07	2.68
$^1D_{CH}$ (96)	1.46 ± 0.04	1.46
$^1D_{CH}$ cat.2 (30)	4.59 ± 0.25	4.50
$^1D_{C'N}$ (46)	0.62 ± 0.01	0.60
$^1D_{C'N}$ cat. 2 (28)	0.76 ± 0.03	0.73
$^2D_{C'NH}$ (50)	0.79 ± 0.02	0.76
$^2D_{C'NH}$ cat.2 (18)	1.78 ± 0.0.13	1.63
$^1D_{C\alpha C'}$ (104)	0.52 ± 0.01	0.52
$^1D_{C\alpha C'}$ cat. 2 (36)	1.14 ± 0.03	1.15
RMSDs from dihedral restraints (°) (330)	3.59 ± 0.10	3.71
Deviations from idealized covalent geometry		
Bonds (Å)	0.003 ± 0.0001	0.003
Angles (°)	0.474 ± 0.009	0.471
Impropers (°)	0.398 ± 0.007	0.392
Lennard–Jones potential energy (kcal/mol) [b]	−793 ± 26	−828
% Residues in most favorable region of Ramachandran plot	86 ± 1	88
RMSDs to the mean structure (Å) [c]		
Ordered backbone residues (2–84)	0.29 ± 0.04	0.30
Ordered heavy atoms (2–84)	0.99 ± 0.06	1.05
Ordered backbone residues (1–88)	0.39 ± 0.08	0.38
Ordered heavy atoms (1–88)	1.11 ± 0.10	1.10

[a] ⟨20⟩ are the ensemble of 20 simulated annealing (SA) structures. The best was chosen based on its lowest energy value. For the ⟨20⟩, values shown are mean ± standard deviation. The final force constants of the target function employed in the SA protocol were: 1,000 kcal mol^{-1} Å^{-2} for bond lengths, 500 kcal mol^{-1} rad^{-2} for angles and improper torsions, 4 kcal mol^{-1} Å^{-4} for the quartic van der Waals (vdW) repulsion term (hard sphere effective vdW radii set to 0.80 times their value in the CHARMM parameters), 50 kcal mol^{-1} Å^{-2} for experimental distance restraints, 50 kcal mol^{-1} rad^{-2} for (ϕ,ψ) dihedral angle restraints, 100 kcal mol^{-1} Å^{-2} for noncrystallographic symmetry, and 1.0 kcal mol^{-1} Å^{-2} for distance symmetry restraints. The force constants (in kcal/Hz^2) used for the higher/lower quality dipolar coupling restraints were as follows: 0.44/0.11 for ^{15}N–^{1}H^N; 0.33/0.11 for ^{13}C$^\alpha$–^{1}H$^\alpha$; 2.0/0.5 for ^{13}C′–^{15}N; 1.5/0.4 for ^{13}C′–^{1}H^N; 4.0/1.0 for ^{13}C$^\alpha$–^{13}C′. A dipolar coupling was assigned the lower force constant value if any overlap in its measurement was observed or for weak cross peaks.

[b] The Lennard–Jones van der Waals energy was calculated using the CHARMM parameters and was not employed in any stage of structure determination.

[c] Backbone calculations included C$^\alpha$, N, and C′ atoms. Ordered residues included 1–88 because no long-range NOEs were observed for residues 89–91. Statistics for residues 2–84 are also included because correlations for residues 1 and 85–87 are either very weak or not observed due to conformational averaging.

rather far from that found for a preliminary low resolution structure of apo-calcyclin (Tables 2, 3).

The Ca^{2+}-dependent conformational change in S100B($\beta\beta$) and implications for target protein binding

No significant differences between the structure of apo-S100B($\beta\beta$) determined here and Ca^{2+}-loaded S100B($\beta\beta$) (Drohat et al., 1998; Matsumura et al., 1998) were observed when the orientation of helices (1, 1′, 4, or 4′) in the X-type four helical bundle dimer interface are compared. Furthermore, the interhelical angles between helices 1 and 2 in the pseudo-EF hand are identical in the presence and absence of Ca^{2+} (refined apo-: 133 ± 1°; Ca^{2+}-bound: 137 ± 5°) (Fig. 5). The absence of a conformational change in the pseudo-EF hand is not surprising because the position of helix 1 is severely restricted by core interactions at the dimer

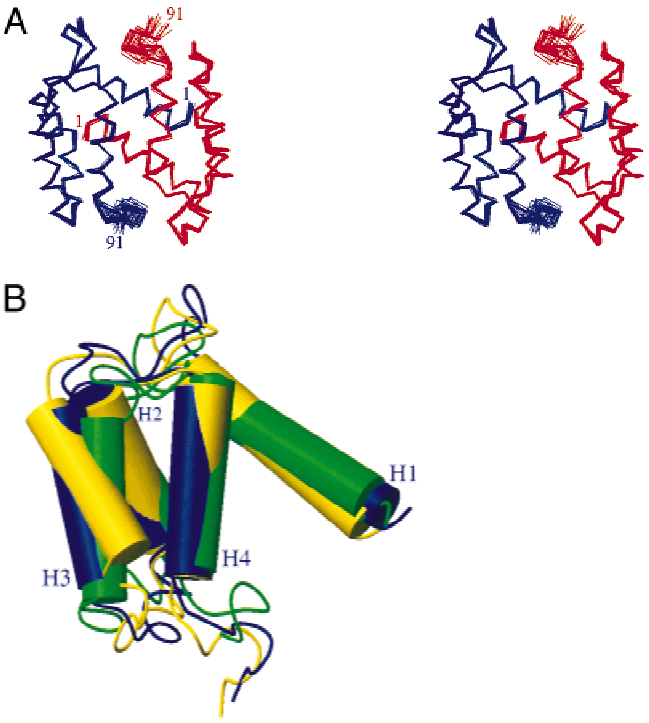

Fig. 4. Structure of rat apo-S100B($\beta\beta$) determined using dipolar coupling restraints. **A:** Stereo view of 20 structures of dimeric apo-S100B($\beta\beta$) aligned by C_α superposition with the two S100β subunits shown in blue and red. The statistical parameters for the structures are given in Table 1. **B:** A comparison of rat apo-S100B($\beta\beta$) determined with dipolar coupling restraints (blue) to previously determined structures of S100B($\beta\beta$) from rat (yellow) (Drohat et al., 1996) and bovine (green) (Kilby et al., 1996). Helices are shown as cylinders, and only a single S100β subunit is illustrated for each structure. In **B**, the S100β subunits were aligned (C_α atoms) using residues 2–49 and 63–84 such that helix 3 was not included in the alignment.

interface in both the presence and absence of Ca^{2+}. In the second EF-hand (the typical EF-hand), there is a large change in the position of helix 3 (~90°) observed upon the addition of Ca^{2+} as judged by differences in the helix 3/helix 4 interhelical angles (Ca^{2+}-bound: $^{NMR}\Omega_{3/4} = 106 \pm 4°$, $^{X\text{-ray}}\Omega_{3/4} = 101$; apo-: $^{new}\Omega_{3/4} = 194 \pm 1°$). As expected, the magnitude of the conformational change is less by 26° than that previously reported for rat apo-S100B($\beta\beta$) (Drohat et al., 1998), and larger by 30° than that reported for bovine S100B($\beta\beta$) (Matsumura et al., 1998). It should be noted that the X-ray structure of Ca^{2+}-loaded S100B($\beta\beta$) from bovine and the NMR structure from rat are nearly indistinguishable with regard to all of their interhelical angles (Table 3) (Drohat et al., 1998; Matsumura et al., 1998).

Based on the higher resolution structure of apo-S100B($\beta\beta$) determined here and the Ca^{2+}-loaded structures of S100B($\beta\beta$), determined by both X-ray crystallography and NMR spectroscopy, we can now more accurately describe the Ca^{2+}-dependent conformational change that is required for S100B to bind target proteins. Interestingly, this conformational change exposes a cleft defined by residues in the hinge region, the C-terminal loop, and helix 3, which is absent in the apo-structure (Fig. 5). This surface on Ca^{2+}-bound S100B($\beta\beta$) is likely to be important for target protein binding because significant changes in chemical shift ($\Delta\delta_{HN} >$ 0.2 ppm; $\Delta\delta_{15N} > 1.0$ ppm) and several intermolecular NOE correlations are observed for residues in this region when a peptide derived from p53 is titrated into the NMR sample containing Ca^{2+}-bound S100B($\beta\beta$). These changes in chemical shift and intermolecular NOE correlations are not observed in titrations of the apo-S100B($\beta\beta$) protein with p53, which demonstrates the Ca^{2+}-dependence of this biologically important interaction (Rustandi et al., 1998).

Materials and methods

Materials

All buffers were passed through Chelex-100 resin (BioRad) to remove trace metals. Perdeuterated Tris, d_{11}-Tris (1 M solution in D_2O, >98.7 atom% deuterium) was purchased from C/D/N Isotopes, Inc. (Vandreuil, Quebec), and D_2O (100.0 atom% deuterium, low in paramagnetic impurities) was purchased from Aldrich Chemical Company (Milwaukee, Wisconsin). $^{15}NH_4Cl$ (>99%) and ^{13}C-labeled glucose were purchased from Cambridge Isotope Laboratories (Woburn, Massachusetts).

Sample preparation

Recombinant S100B($\beta\beta$) was overexpressed in *Escherichia coli* strain HMS174(DE3) transformed with an expression plasmid containing the rat S100β gene. Unlabeled, ^{15}N-labeled, and ^{13}C,^{15}N-labeled S100B($\beta\beta$) were prepared and purified (>99%) under reducing conditions using procedures similar to those described previously (Amburgey et al., 1995b; Drohat et al., 1996, 1998), except that 0.5 mM DTT (Gibco BRL) was used as a reducing agent throughout the preparation instead of β-mercaptoethanol. The reported subunit concentrations of S100B($\beta\beta$) were determined using a BCA protein assay with an S100B($\beta\beta$) standard of known subunit concentration as previously described (Drohat et al., 1996, 1998).

Conditions for the NMR samples were 1.0–1.5 mM (subunit concentration) ^{15}N-, or ^{13}C,^{15}N-labeled S100B($\beta\beta$), 0.34 mM NaN_3, 5 mM DTT, 5–10% D_2O, 6–10 mM d_{11}-Tris-HCl, pH 6.5, and sufficient NaCl (17–20 mM) to give an ionic strength equal to 25 mM at 25 or 38 °C. The liquid-crystalline (LC) medium, comprising a mixture (3:1) of dimyristoyl phosphatidylcholine (DMPC) and dihexanoyl phosphatidylcholine (DHPC) bicelles (Sanders, 1992), was added to 4% w/v as described (Ottiger & Bax, 1998). For an isotropic control, a separate sample was prepared using the same conditions except without phospholipids.

NMR spectroscopy

A 3D CT-(H)CA(CO)NH experiment was collected without H^α decoupling during C^α acquisition in t_2 to record C^α-H^α splittings (Tjandra & Bax, 1997b). This data set was recorded with 45* × 64* × 512* points (* indicates complex points), and acquisition times of 27.0 ms (^{15}N), 25.3 ms (^{13}C), and 56.1 ms (^{1}H) in t_1, t_2, and t_3, respectively. The carrier positions were 117.1 and 56.0 ppm for ^{15}N and ^{13}C, and the processed data consisted of 128 × 512 × 1,024 real points in F1, F2, and F3, respectively. A semi-constant time ^{1}H-^{15}N HSQC (Ottiger et al., 1998) was collected without $^{13}C'$ decoupling but with composite pulse decoupling during t_1 to obtain very high resolution in $^{13}C'$-^{15}N splittings. These data were

Table 2. *Comparison of S100 structures*

Backbone C^{α} RMSD (Å)	Rat apo-S100B[a]	Bovine apo-S100B[b]	apo-calcyclin[c]	Rat Ca^{2+}-S100B[d]	Helices 1,2,4 rat Ca^{2+}-S100B[e]
Rat apo-S100B with dipolar couplings	2.54	3.43	3.32	5.07	1.52
Rat apo-S100B[a]	0.00	3.48	4.07	5.62	2.02
Bovine apo-S100B[b]	3.48	0.00	3.14	4.35	2.20
Apo-calcyclin[c]	4.07	3.14	0.00	3.83	1.60

[a]Residues 2–84 from coordinates of the solution structure of rat apo-S100B($\beta\beta$) with PDB accession code 1SYM (Drohat et al., 1996) are compared.
[b]Residues 2–84 from coordinates of the solution structure of bovine apo-S100B($\beta\beta$) with PDB accession code 1CFP (Kilby et al., 1996) are compared.
[c]Residues 4–44 and 50–84 from coordinates of the solution structure of apo-calcyclin with PDB accession code 1CNP (Potts et al., 1995) are compared.
[d]Residues 2–84 from coordinates of the solution structure of rat Ca^{2+}-bound S100B($\beta\beta$) with PDB accession code 1QLK (Drohat et al., 1998) are compared.
[e]Residues 2–18, 29–40, and 70–83 from coordinates of the solution structure of rat apo-S100B($\beta\beta$) with PDB accession code 1QLK (Drohat et al., 1998) are compared. For comparisons to calcyclin, residues 4–20, 31–42, and 70–83 of calcyclin were used. In each case, a single subunit of an average structure from a group of acceptable structures was used in the calculation.

acquired with 200* × 512* points in t_1 and t_2, with acquisition times of 110 ms (^{15}N) and 63.9 ms (^{1}H), and with carrier frequencies set to 119.4 (^{15}N) and 177.0 ($^{13}C'$) ppm. The processed matrix contained 2,048 × 4,096 real points in F1 and F2, respectively. A 2D IPAP ^{1}H-^{15}N HSQC (Ottiger et al., 1998) was collected with the ^{15}N carrier positioned at 118.9 ppm and the ^{13}C carrier switched between 56.0 and 177.0 ppm for C_{α} and C' pulses, respectively. The data were separated into complementary in-phase and anti-phase matrices, each with 200* × 1,024* points in t_1 and t_2, and acquisition times of 82.2 ms (^{15}N) and 122.1 ms (^{1}H). The processed matrices contained 2,048 × 2,048 real points in F1 and F2. A 3D CT HNCO (Grzesiek & Bax, 1993) without C^{α} decoupling during $^{13}C'$ acquisition in t_2 was collected for measuring H^{N}-N and C^{α}-C' splittings, respectively. In this experiment, 42* × 32* × 512* points were recorded with carrier frequencies of 116.8 (^{15}N) and 176.9 ($^{13}C'$) ppm. The acquisition times were 26.9 ms (^{13}C), 26.9 ms (^{15}N), and 60.2 ms (^{1}H), and the final processed matrix consisted of 1,024 × 128 × 1,024 real points in F1, F2, and F3. All data were collected on 600 MHz Bruker Avance series DMX spectrometers, equipped with five frequency channels and

Table 3. *Interhelical angles of EF-hands in S100 Ca^{2+}-binding proteins*[a]

Helices	Refined apo-S100B[b,c]	Rat apo-S100B[b,c]	Bovine apo-S100B[d]	Apo-calcyclin[e]	Apo-calbindin[f]	Ca^{2+}-calcyclin[b,g]	Ca^{2+}-calbindin[h]	Human Ca^{2+}-S100B[b,i]	Bovine Ca^{2+} S100B[j]	Rat Ca^{2+}-S100B[b,c]
I–II	$133 \pm 1^{\perp}$	$135 \pm 3^{\perp}$	$130 \pm 3^{\perp}$	$126 \pm 27^{\perp}$	$123 \pm 3^{\perp}$	$110 \pm 8^{\perp}$	$128^{\perp}$	$138 \pm 4^{\perp}$	$135^{\perp}$	$137 \pm 5^{\perp}$
I–III	$-46 \pm 1^{\parallel}$	$-22 \pm 2^{\parallel}$	$-66 \pm 2^{\parallel}$	$-83 \pm 22^{\perp}$	$-109 \pm 9^{\perp}$	$-81 \pm 16^{\perp}$	$-113^{\perp}$	$-86 \pm 5^{\perp}$	—	$-118 \pm 5^{\perp}$
I–IV	$120 \pm 1^{\perp}$	$121 \pm 2^{\perp}$	$119 \pm 2^{\perp}$	$119 \pm 17^{\perp}$	$128 \pm 4^{\perp}$	$126 \pm 5^{\perp}$	$120^{k\perp}$	$113 \pm 2^{\perp}$	$127^{\perp}$	$128 \pm 4^{\perp}$
II–III	$149 \pm 1^{\parallel}$	$138 \pm 4^{\parallel}$	$144 \pm 3^{\parallel}$	$144 \pm 15^{\parallel}$	$124 \pm 7^{\perp}$	$161 \pm 10^{\parallel}$	$113^{\perp}$	$133 \pm 4^{\parallel}$	$97^{\perp}$	$104 \pm 3^{\perp}$
II–IV	$-40 \pm 1^{\parallel}$	$-36 \pm 2^{\parallel}$	$-46 \pm 3^{\perp}$	$-16 \pm 10^{\parallel}$	$-34 \pm 4^{\parallel}$	$-36 \pm 13^{\parallel}$	$-28^{k\parallel}$	$-46 \pm 2^{\parallel}$	—	$-35 \pm 4^{\parallel}$
III–IV	$-166 \pm 1^{\parallel}$	$-140 \pm 4^{\parallel}$	$164 \pm 4^{\parallel}$	$145 \pm 16^{\parallel}$	$118 \pm 8^{\perp}$	$135 \pm 12^{\perp}$	$126^{k\perp}$	$148 \pm 4^{\parallel}$	$101^{\perp}$	$106 \pm 4^{\perp}$

[a]Interhelical angles (Ω) range from $-180°$ to $+180°$ and are classified as either: parallel ($\parallel$) for $0° \leq |\Omega| \leq 40°$ and $140° \leq |\Omega| \leq 180°$, or as perpendicular ($\perp$) for $40° < |\Omega| < 140°$, as described (Harris et al., 1994). The sign (+ or −) of Ω can be determined by: (1) orienting the molecule such that the two helices of interest (i,j) are in planes parallel to the screen with the first helix (i) in front of the second (j) and the first helix (i) aligned vertically (0°, with its N → C vector pointing upward), (2) aligning an imaginary vector vertically (0°) with its tail placed at the N-terminus of the second helix (j) and rotating it (by (180° clockwise or counterclockwise) to align with the N → C vector of the second helix (j) where a clockwise rotation gives a positive (+) Ω value and a counterclockwise rotation gives a negative (−) Ω value.
[b]Interhelical angles were calculated using the program Iha 1.4.
[c]Helices in rat apo-S100B are helix I (2–18), helix II (29–40), helix III (50–63), and helix IV (70–83) (Drohat et al., 1996), and helices in Ca^{2+}-loaded S100B are helix I (2–20), helix II (29–38), helix III (50–61), and helix IV (70–83).
[d]Helices in bovine apo-S100B are helix I (2–18), helix II (29–38), helix III (50–62), and helix IV (70–84) (Kilby et al., 1996).
[e]Helices in apo-calcyclin are helix I (4–16), helix II (32–42), helix III (53–62), helix IV (70–85) (Potts et al., 1995).
[f]Helices in apo-calbindin are helix I (3–13), helix II (25–35), helix III (46–54), helix IV (63–72) (Skelton et al., 1990).
[g]Helices in Ca^{2+}-calcyclin were defined as helix I (5–20), helix II (30–41), helix III (50–61), and helix IV (70–83) (Sastry et al., 1998).
[h]Taken from Szebenyi and Moffat (1986).
[i]Helices in human Ca^{2+}-S100B were defined as helix I (2–17), helix II (30–39), helix III (52–58), and helix IV (70–87); this NMR sample contained 10% TFE (Smith & Shaw, 1998).
[j]Taken from Matsumura et al. (1998).
[k]The angle was taken from the center portion of the bent helix IV in calbindin as described in Szebenyi & Moffat (1986).

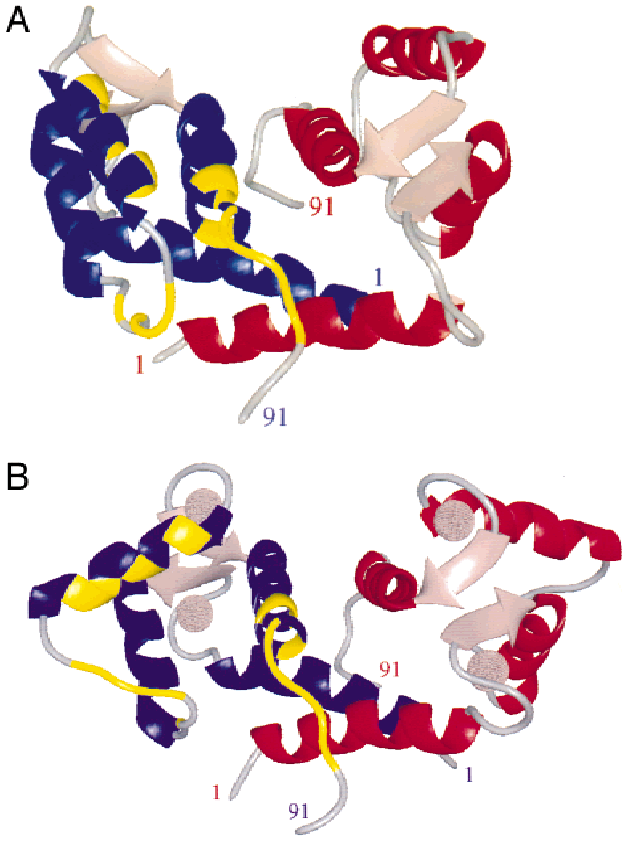

Fig. 5. Comparison of the three-dimensional structures of (**A**) apo-S100B($\beta\beta$) determined with dipolar coupling constraints and (**B**) Ca^{2+}-bound S100B($\beta\beta$) from rat (Drohat et al., 1998). Shown in yellow are regions of the protein that change in chemical shift ($H^N > 0.2$ ppm) when a peptide derived from p53 is titrated into Ca^{2+}-loaded S100B($\beta\beta$) (Rustandi et al., 1998). In this complex, two peptides bind per S100B($\beta\beta$) dimer and residues in each subunit are affected equally, but for clarity, only residues on one of the two subunits are highlighted (in yellow).

a triple resonance, triple-axis gradient 5-mm probehead. Pulse field gradients were used in each of the 2D pulse sequences for artifact elimination (Bax & Pochapsky, 1992) and WATERGATE solvent signal suppression (Piotto et al., 1992). In the 3D CT-(H)CA(CO)NH and 3D CT-HNCO experiments, pulsed field gradients were additionally used for coherence selection (Kay et al., 1992). In all experiments the ^1H carrier was set on water. Data were collected in liquid crystalline media under isotropic (25 °C) and anisotropic (38 °C) conditions, and additional isotropic data were collected at 38 °C in a sample that did not contain the phospholipid mixture. In the final processed data, the peak positions were determined using the contour averaging method with the data analysis program PIPP (Garrett et al., 1991).

Structure calculations

Interproton distance restraints were previously derived from 2D, 3D, and 4D NOESY and ROESY experiments (Amburgey et al., 1995b; Drohat et al., 1996), and were classified on the basis of peak intensity into categories with lower bounds of 1.8 Å and upper bounds of 2.7 Å (2.9 for H^N), 3.3 Å (3.5 Å for H^N), 4.2 Å, 5.0 Å, and 6.0 Å as previously described (Clore et al., 1986). Distances for degenerate or nonstereospecifically assigned protons were represented using an $(\Sigma r^{-6})^{-1/6}$ sum (Nilges, 1993) instead of center averaging as was used in the previous structure calculation of apo-S100B (Drohat et al., 1996). For the residues that exhibited multiple H^N resonances (Amburgey et al., 1995b), distance restraints or dipolar coupling restraints were employed only for those H^N NOEs or dipolar couplings where similar effects were observed at each of the two chemical shifts (Drohat et al., 1996). Backbone dihedral angle restraints were determined on the basis of $^3J_{HNH\alpha}$ couplings from the HNHA experiment (Vuister & Bax, 1993), and from chemical shift and sequence homologies with triplets of residues in a library of proteins for which high resolution crystal structures and chemical shifts are known (G. Cornilescu, F. Delaglio, A. Bax, unpubl. obs.). Backbone hydrogen bond restraints of $r_{NH\text{-}O} = 1.5$–2.8 Å and $r_{N\text{-}O} = 2.4$–3.5 Å were used in regions of regular secondary structure (Wüthrich, 1986).

The internuclear dipolar couplings (in hertz) were determined from the difference in J splitting between the isotropic and aligned phases and were grouped into two categories on the basis of peak quality. A modified version of the X-PLOR program incorporated a pseudo-potential for dipolar coupling information and was used to calculate the structures (Brünger, 1992; Clore et al., 1998b). In short, the protocol uses a pseudo external axis system that was defined by creating a tetra-atomic molecule containing atoms X, Y, Z, and O, which are constrained by three perpendicular bonds O–X, O–Y, and O–Z. These three bonds represent the *x*, *y*, and *z* axes of the alignment tensor **A**. To avoid any possible direct interaction between the axis system and the molecule of interest, the external axis system was placed far (50–100 Å) away from the protein. In addition, the atom O, which defines the origin, was constrained to the lattice using a harmonic potential, while the orientation of the axis system was allowed to float freely during the structure calculation. The $E_{dipolar}$ was evaluated by calculating the cylindrical angles θ and ϕ between the appropriate dipolar interaction vector (N–H, C^α–H^α, H^N–C′, etc.) and the external axis system. The axial ($\mathbf{A}_a$) and rhombic ($\mathbf{A}_r$) components of **A** were obtained from a histogram of the dipolar couplings as described previously (Clore et al., 1998a). The force constants for the dipolar coupling energies were slowly increased in concert with the force constant of the NOE energy during the cooling stage of the structure calculations. The initial force constants used were typically very small (0.001 kcal Hz^{-2}), and the final force constants were determined for each of the five sets of dipolar couplings such that the calculated structures represented the estimated uncertainty in each dipolar coupling data set. These are ca. 1.5 Hz for the good category (category 1) D_{NH} and D_{CH} couplings, 2.5 and 5 Hz for the less resolved category (category 2) D_{NH} and D_{CH} couplings, respectively; 0.5 and 1 Hz for the category 1 and 2 $D_{C'N}$ couplings, 1 and 2 Hz for the category 1 and 2 $^2D_{C'HN}$ couplings, and 0.5 and 1 Hz for category 1 and 2 $D_{C'C\alpha}$ couplings. The final force constants used in the structure calculations were 0.44/0.11, 0.33/0.11, 2.0/0.5, 1.5/0.4, and 4.0/1.0 kcal Hz^{-2} for the ^{15}N–H^N, C^α–H^α, C′–N, C′–H^N, and C^α–C′ dipolar couplings in categories 1 and 2, respectively (Table 1). As the NMR spectrum indicates a S100B($\beta\beta$) dimer to be fully symmetric, noncrystallographic symmetry (NCS) and distance symmetry restraints were also used, with force constants of 100 kcal/mol $Å^2$ and 1.0 kcal/mol $Å^2$, respectively (Nilges, 1993). Of the 100 structures calculated, 20 were selected based on their lowest total energies.

Note added in proof

Since the submission of this manuscript, a high resolution structure for apo-calcyclin has been reported. This newly refined apo-calcyclin structure is in better agreement with the structure reported here than the apo-calcyclin structure reported previously (Potts et al., 1995).

Acknowledgments

We are grateful to Dr. Ad Bax for his help in collecting the NMR data and for very useful discussions. This work was supported in part by a National Institutes of Health grant (R01GM58888 to D.J.W.) and American Cancer Society Grant (JFRA-641 to D.J.W.), and by SRIS and DRIF funding from the University of Maryland School of Medicine and the State of Maryland (to D.J.W.). This study made use of a 600 MHz NMR spectrometer in the UMB NMR facility that was purchased with funds from the University of Maryland and the NIH shared instrumentation grant program (S10RR10441 to D.J.W.). We are also grateful to Dr. Stéphane Gagné for a program, Iha 1.4, which calculates interhelical angles.

References

Albert KA, Wu WC-S, Nairn AC, Greengard P. 1984. Inhibition by calmodulin of calcium/phospholipid-dependent protein phosphorylation. *Proc Natl Acad Sci USA 81*:3622–3625.

Amburgey JC, Abildgaard F, Starich MR, Shag S, Hilt DC, Weber DJ. 1995a. ^{1}H, ^{13}C, and ^{15}N resonance assignments and secondary structure of S100β by NMR spectroscopy. *FASEB J 9*:A1430.

Amburgey JC, Abildgaard F, Starich MR, Shah S, Hilt DC, Weber DJ. 1995b. ^{1}H, ^{13}C, ^{15}N NMR assignments and solution secondary structure of rat apo-S100β. *J Biomol NMR 6*:171–179.

Baudier J, Bronner C, Kligman D, Cole RD. 1989. Protein kinase C substrates from bovine brain. *J Biol Chem 264*:1824–828.

Baudier J, Delphin C, Grundwald D, Khochbin S, Lawrence JJ. 1992. Characterization of the tumor suppresor protein p53 as a protein kinase C substrate and a S100B-binding protein. *Proc Natl Acad Sci USA 89*:11627–11631.

Bax A, Pochapsky SS. 1992. Optimized recording of heteronuclear multidimensional NMR spectra using pulsed field gradients. *J Magn Reson 99*:638–643.

Bax A, Tjandra N. 1997. High resolution NMR structure of human ubiquitin in an aqueous liquid crystalline medium. *J Biomol NMR 10*:289–292.

Bianchi R, Giambanco I, Donato R. 1993. S100 protein, but not calmodulin, binds to glial fibrillary acidic protein and inhibits its polymerization in a Ca^{+2}-dependent manner. *J Biol Chem 268*:12669–12674.

Brünger AT. 1992. *XPLOR version 3.1*. New Haven, Connecticut: Yale University Press.

Brünger AT, Clore GM, Gronenborn AM, Saffrich R, Nilges M. 1993. Assessing the quality of solution nuclear magnetic resonance structures by complete cross-validation. *Science 261*:328–331.

Clore GM, Gronenborn AM, Bax A. 1998a. A robust method for determining the magnitude of fully asymmetric alignment tensor of oriented macromolecules in the absence of structural information. *J Magn Reson 133*:216–221.

Clore GM, Gronenborn AM, Tjandra N. 1998b. Direct structure refinement against dipolar couplings in the presence of rhombicity of unknown magnitude. *J Magn Reson 131*:159–162.

Clore GM, Nilges M, Sukumaran DK, Brünger AT, Karplus M, Gronenborn AM. 1986. The three-dimensional structure of a 1-purothionin in solution: Combined use of nuclear magnetic resonance, distance geometry, and restrained molecular dynamics. *EMBO J 5*:2729–2735.

Clore GM, Omichinski JG, Sakaguchi K, Zambrano N, Sakamoto H, Appella E, Gronenborn GM. 1995. Interhelical angles in the solution structure of the oligomerization domain of p53: Correction. *Science 267*:1515–1516.

Cornilescu GC, Marquardt JL, Ottiger M, Bax A. 1998. Validation of protein structure from anisotropic carbonyl chemical shifts in a dilute liquied crystalline phase. *J Am Chem Soc 120*:6836–6837.

Donato R. 1991. Perspectives in S-100 protein biology. *Cell Calcium 12*:713–726.

Drohat AC, Amburgey JC, Abildgaard F, Starich MR, Baldisseri D, Weber DJ. 1996. Solution structure of rat apo-S100B($\beta\beta$) as determined by NMR spectroscopy. *Biochemistry 35*:11577–11588.

Drohat AC, Baldisseri DM, Rustandi RR, Weber DJ. 1998. Solution structure of calcium-bound rat S100B($\beta\beta$) as determined by NMR spectroscopy. *Biochemistry 37*:2729–2740.

Garrett DS, Powers R, Gronenborn AM, Clore GM. 1991. A common sense approach to peak picking in two-, three-, and four-dimensional spectra using automatic computer analysis of contour diagrams. *J Magn Reson 95*:214–220.

Groves P, Finn BE, Kuznicki J, Forsen S. 1998. A model for target protein binding to calcium-activated S100 dimers. *FEBS Lett 421*:175–179.

Grzesiek S, Bax A. 1992. Improved 3D triple-resonance NMR techniques applied to a 31 kDa protein. *J Magn Reson 96*:432–440.

Grzesiek S, Bax A. 1993. Amino acid type determination in the sequential assignment process of uniformly ^{13}C/^{15}N-enriched proteins. *J Biomol NMR 3*:185–204.

Harris NL, Resnell SR, Cohen FE. 1994. Four helix bundle diversity in globular proteins. *J Mol Biol 236*:1356–1368.

Kay LE, Keifer P, Saarinen T. 1992. Pure absorption gradient enhanced heteronuclear single quantum correlation spectroscopy with improved sensitivity. *J Am Chem Soc 114*:10663–10665.

Kilby PM, Van Eldik LJ, Roberts GCK. 1996. The solution structure of the bovine S100B protein dimer in the calcium-free state. *Structure 4*:1041–1052.

Kligman D, Hilt D. 1988. The S100 protein family. *Trends Biochem Sci 13*:437–443.

Laskowski RA, MacArthur MW, Moss DS, Thornton JM. 1993. PROCHECK: A program to check the stereochemical quality of protein structures. *J Appl Crystallogr 26*:283–291.

Matsumura H, Shiba T, Inoue T, Harada S, Kai Y. 1998. A novel mode of target recognition suggested by the 2.0 Å structure of holo S100B from bovine brain. *Structure 6*:233–241.

Nilges M. 1993. A calculation strategy for the structure determination of symmetric dimers by ^{1}H NMR. *Proteins Struct Funct Genet 17*:297–309.

Ottiger M, Bax A. 1998. Bicelle-based liquid crystals for NMR-measurement of dipolar couplings at acidic and basic pH values. *J Biomol NMR*. In press.

Ottiger M, Delaglio F, Bax A. 1998. Measurement of J and dipolar couplings from simplified two-dimensional NMR spectra. *J Magn Reson 131*:373–378.

Patel J, Kligman D. 1987. Purification and characterization of an Mr 87,000 protein kinase C substrate from rat brain. *J Biol Chem 262*:16686–16691.

Patel J, Marangos PJ, Heydorn WE, Chang G, Verma A, Jacobowitz D. 1983. S-100-mediated inhibition of brain protein phosphorylation. *J Neurochem 41*:1040–1045.

Piotto M, Saudek V, Sklenar V. 1992. Gradient-tailored excitation for single-quantum NMR spectroscopy of aqueous solutions. *J Biomol NMR 2*:661–665.

Potts BCM, Smith J, Akke M, Macke TJ, Okazaki K, Hidaka H, Case DA, Chazin WJ. 1995. The structure of calcyclin reveals a novel homodimeric fold for S100 Ca-binding proteins. *Nat Struct Biol 2*:790–796.

Rustandi RR, Drohat AD, Baldisseri DM, Wilder PT, Weber DJ. 1998. The Ca^{+2}-dependent interaction of S100B($\beta\beta$) with a peptide derived from p53. *Biochemistry 37*:1951–1960.

Sanders CR, Schwonek JP. 1992. Characterization of magnetically orientable bilayers in mixtures of dihexanoylphosphatidylcholine and dimyristoylphosphatidylcholine by solid-state NMR. *Biochemistry 31*:8898–8905.

Sastry M, Ketchem RR, Crescenzi O, Weber C, Lubienski MJ, Hidaka H, Chazin WJ. 1998. The three-dimensional structure of Ca^{2+}-bound calcyclin: Implications for Ca^{2+}-signal transduction by S100 proteins. *Structure 6*:223–231.

Schafer BW, Heizmann CW. 1996. The S100 family of EF-hand calcium-binding proteins: Functions and pathology. *Trends Biochem Sci 21*:134–140.

Skelton NJ, Forsen S, Chazin WJ. 1990. ^{1}H NMR resonance assignments, secondary structure, and global fold of apo bovine calbindin D_{9K}. *Biochemistry 29*:5752–5761.

Smith SP, Shaw GS. 1998. A novel calcium-sensitive switch revealed by the structure of human S100B in the calcium-bound form. *Structure 6*:211–222.

Strynadka NCJ, James MNG. 1989. Crystal structures of the helix-loop-helix calcium-binding proteins. *Annu Rev Biochem 58*:951–998.

Stumpo DJ, Graff JG, Albert KA, Greengard P, Blackshear PJ. 1989. Molecular cloning, characterization, and expression of cDNA encoding the "80- to 87-kDa" myristoylated alanine-rich C kinase substrate: A major cellular substrate for protein kinase C. *Proc Natl Acad Sci USA 86*:4012–4016.

Szebenyi DME, Moffat K. 1986. The refined structure of vitamin D-dependent calcium binding protein from bovine intestine-molecular details, ion binding, and implications for the structure of other calcium-binding proteins. *J Biol Chem 261*:8761–8777.

Tjandra N, Bax A. 1997a. Direct measurement of distances and angles in biomolecules by NMR in a dilute liquid crystalline medium. *Science 278*:1111–1114.

Tjandra N, Bax A. 1997b. Large variations in ^{13}Cα chemical shift anisotropy in proteins correlate with secondary structure. *J Am Chem Soc 119*:9576–9577.

Tjandra N, Grzesiek S, Bax A. 1996. Magnetic field dependence of nitrogen-proton J splittings in ^{15}N-enriched human ubiquitin resulting from relaxation interference and residual dipolar coupling. *J Am Chem Soc 118*:6264–6272.

Tjandra N, Omichinski JG, Gronenborn AM, Clore GM, Bax A. 1997. Use of dipolar ^{1}H-^{15}N and ^{1}H-^{13}C couplings in the structure determination of magnetically oriented macromolecules in solution. *Nat Struct Biol 4*:732–738.

Tolman JR, Flanagan JM, Kennedy MA, Prestegard JH. 1995. Nuclear magnetic dipolar interactions in field-oriented proteins: Information for structure determination in solution. *Proc Natl Acad Sci USA 92*:9279.

Urbauer JL, Short JH, Dow LK, Wand JW. 1995. Structural analysis of a novel interaction by calmodulin: High-affinity binding of a peptide in the absence of calcium. *Biochemistry 34*:8099–8109.

Vuister GW, Bax A. 1993. Quantitative J correlation: A new approach for measuring homonuclear three-bond J(HNHα) coupling constants in 15-N enriched proteins. *J Am Chem Soc 115*:7772–7777.

Wilder PT, Rustandi RR, Drohat AC, Weber DJ. 1998. S100B($\beta\beta$) inhibits the protein kinase C-dependent phosphorylation of a peptide derived from p53 in a Ca-dependent manner. *Protein Sci 7*:794–798.

Wüthrich K. 1986. *NMR of proteins and nucleic acids*. New York: John Wiley.

Zimmer DB, Cornwall EH, Landar A, Song W. 1995. The S100 protein family: history, function, and expression. *Brain Res Bull 37*:417–429.